# Resolution of the 66-Fold Superstructure of $DySe_{1.84}$ by X-ray Diffraction and Second-Moment Scaled Hückel Calculations

A. van der Lee,† L. M. Hoistad, and M. Evain*

*Institut des Matériaux de Nantes, UMR-CNRS 110, Laboratoire de Chimie des Solides, 2, rue de la Houssinière, B.P. 3229, 44322 Nantes Cedex 3, France*

B. J. Foran and S. Lee*

*Willard H. Dow Laboratories, Department of Chemistry, Ann Arbor, Michigan 48109-1055*

*Received May 29, 1996. Revised Manuscript Received September 17, 1996*[⊗]

We report the superlattice of the modulated structure $DySe_{1.84}$. The modulation is of the charge density wave type, associated with electronic states on selenium atoms arranged in two-dimensional square nets. The complete modulated structure can be described in the superspace group formalism in a 3+2 dimensional space group $C_{c\bar{m}\bar{m}1}^{Pm2_1n}$. The basic cell observed by single-crystal X-ray diffraction is orthorhombic with $a = 3.9912(3)$ Å, $b = 3.9863(1)$ Å, and $c = 8.206(1)$ Å. The modulation wave vectors are $\mathbf{q}_1 = \alpha\mathbf{a}^* + \beta\mathbf{b}^* + {}^1/_2\mathbf{c}^*$ and $\mathbf{q}_2 = \alpha\mathbf{a}^* - \beta\mathbf{b}^* + {}^1/_2\mathbf{c}^*$, where $\alpha = 0.33338(16)$ and $\beta = 0.27284(6)$. Structure refinement based on first- and second-order satellites as well as main lattice reflections produced solutions in four different space groups that could not be differentiated on the basis of agreement factors. A best solution was sought by use of second-moment scaled, tight-binding band calculations. The lowest energy model found was similar to but not identical with two of those refined for X-ray data. This lowest energy structure can be rationalized by analysis of second-nearest-neighbor interactions within the selenium square nets.

## Introduction

Crystalline structures with highly anisotropic bonding, i.e., low-dimensional materials, have been extensively studied in the past few decades.[1−4] The interest has grown as materials in this class have been found to exhibit high-$T_c$ superconductivity, charge density waves, and intercalation chemistry. For the rare-earth chalcogenides, charge density wave (CDW) modulations as well as site occupancy ordering lead to a range of modulated structures.[5,6] In particular, these modulations can be attributed to the electronic structure of two-dimensional square-nets of selenium atoms. As these phases are insulators, the concept of the covalent bond can be used to account for localized valence electrons. However, the proximity of these structures to the metallic regime encourages a band theoretical treatment in discussions of the electronic structure.

CDWs have been studied extensively in the transition-metal chalcogenides where the CDW is associated with electronic states comprised mainly of transition-metal d orbitals; e.g., $TaS_2$[7,8] and $Mo_2S_3$.[9] The low-dimensional rare-earth chalcogenides are thus very different in that there the CDW is associated with electronic states of the more anionic chalcogen atoms in the lattice. Thus while the metal atoms are subject to displacive modulations in the transition-metal CDW materials, in the rare-earth selenides, the CDW is observed as the displacement of the square sheet selenium atoms.

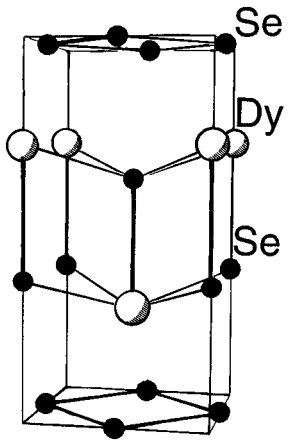


**Figure 1.** Unit cell of the average structure of $Dy_{11}Se_{20}$.

The average structure of the rare-earth dichalcogenides (Figure 1) was deduced from early studies, which also reported several differently sized superlattices.[10] Recent X-ray determinations have allowed the resolution of the superlattice structure for a few of these

* To whom correspondence should be addressed.
† Current address: Laboratoire des Procédés et Matériaux Membranaires, UMR-CNRS 5635, Université de Montpellier II, Place E. Bataillon, 34095 Montpellier Cedex, France.
⊗ Abstract published in *Advance ACS Abstracts,* November 1, 1996.
(1) Wilson, J. A.; DiSalvo, F. J.; Mahajan, S. *Adv. Phys.* **1975**, *24*, 117.
(2) Rouxel, J. Ed. *Crystal Chemistry and Properties of Quasi-One-Dimensional Structures*; Reidel: Dordrecht, 1986.
(3) Levy, F., Ed. *Electronic Structure and Electronic Transitions in Layered Materials*; Reidel: Dordrecht, 1986.
(4) Friend, R. H.; Yoffe, A. D. *Adv. Phys.* **1987**, *36*, 1.
(5) Plambeck-Fischer, P.; Urland, W.; Abriel, W. *Z. Kristallogr.* **1987**, *178*, 182.
(6) Foran, B.; Lee, S.; Aronson, M. C. *Chem. Mater.* **1993**, *5*, 974.
(7) Brouwer, R. *Ph.D. Thesis,* University of Groningen, The Netherlands, 1978.
(8) Yamamoto, A. *Phys. Rev. B* **1983**, *27*, 7823.
(9) Schutte, W. J.; Disselborg, F. J.; De Boer, J. L. *Acta Crystallogr. B* **1993**, *49*, 787.
(10) Wang, R.; Steinfink, H. *Inorg. Chem.* **1967**, *6*, 1687.

S0897-4756(96)00302-X CCC: $14.00 

**Table 1. Crystal Data of $Dy_{11}Se_{20}$ and Conditions of the Data Collection**

| | | | | |
|---|---|---|---|---|
| formula | $Dy_{11Se20}$ | | | |
| formula wt (amu) | 306.05 | | | |
| density (calc) | 7.830 | | | |
| $F(000)$ | 256 | | | |
| linear absorption coefficient ($cm^{-1}$) | 538.7 | | | |
| max correction | 38.89 | | | |
| min correction | 1.72 | | | |
| cryst size | $<0.03 \times 0.035 \times 0.0025$ cm$^3$ | | | |
| superspace group | $C^{Pm2_1n}_{c\bar{m}\bar{m}1}$ | | | |
| basic unit cell | $a = 3.9912(3)$ Å | | | |
| | $b = 3.9863(1)$ Å | | | |
| | $c = 8.206(1)$ Å | | | |
| | vol = 130.56(3) Å$^3$ | | | |
| modulation vectors | $\mathbf{q}_1 = \alpha\mathbf{a}^* + \beta\mathbf{b}^* + {}^1/_2\mathbf{c}^*$ | | | |
| | $\mathbf{q}_1 = \alpha\mathbf{a}^* - \beta\mathbf{b}^* + {}^1/_2\mathbf{c}^*$ | | | |
| | $\alpha = 0.33338(16)$; $\beta = 0.27284(6)$ | | | |
| diffractometer | CAD−4F | | | |
| temp (K) | 295 K | | | |
| radiation | Mo K−$L_{2,3}$ | | | |
| scan mode | $\omega/(2\theta)$ | | | |
| $hkl$mn range | $h_{min}/h_{max}$ | $k_{min}/k_{max}$ | $l_{min}/l_{max}$ | $\theta_{min}/\theta_{max}$ |
| main reflns | 0/7 | −7/7 | −14/14 | 1.5/40.0 |
| 1st-order reflns | 0/6 | 0/6 | −13/13 | 1.5/35.0 |
| 2nd-order reflns | 0/6 | 0/6 | −12/12 | 1.5/30.0 |
| std reflns | $(0\bar{2}0)$, (200), $(0\bar{1}\bar{1})$ every hour | | | |

phases with smaller, commensurate superlattice modulations, on the order of 2−10 times the subcell volume.[5,6] However, the present work offers a study of a much larger superlattice ordering 66× the subcell volume. Some of the present authors previously reported X-ray evidence for an incommensurate superlattice in $DySe_{1.84}$, the same phase discussed in this article, though here it is referred to as $Dy_{11}Se_{20}$ (or even $Dy_{65.3}Se_{120}$). This superlattice was rationalized as due to a CDW state, based on analyses of the electronic structure as studied by extended Hückel band calculations. In particular, a calculated map of the Fermi surface showed nesting vectors matching the incommensurate wave vectors observed on precession X-ray diffraction photographs.[6]

To gain more insight into the structural distortions inherent in this phase, we now make a study of the complete modulated structure of $Dy_{11}Se_{20}$ by combining X-ray crystallography and semiempirical quantum mechanical theoretical methods. The symmetry of this two-dimensionally modulated structure can be conveniently described with a (3+2)$D$ superspace group.[11−13] To discriminate between the different alternative models that emerged from the structural refinements, we calculate the total energy using second-moment scaled Hückel theory.[14−16] The second-moment scaling method has proven its viability for the rationalization of covalent systems, such as the Hume−Rothery electron concentration rules for transition-metal and noble-metal alloys and the late-transition-metal elemental structures.[17−19]

## Experimental Section

The synthesis and crystal growth of $Dy_{11}Se_{20}$ have been described elsewhere.[6] Weissenberg and Buerger photographs confirmed the close to tetragonal symmetry of the basic cell, and clearly indicated the orthorhombic symmetry of the two modulation wave vectors $\mathbf{q}_1 = \alpha\mathbf{a}^* + \beta\mathbf{b}^* + {}^1/_2\mathbf{c}^*$ and $\mathbf{q}_2 = \alpha\mathbf{a}^* - \beta\mathbf{b}^* + {}^1/_2\mathbf{c}^*$. The same good-quality crystal used in the previous study was mounted on a CAD-4F diffractometer and the intensities of 80 first-order satellite reflections were carefully centered. A least-squares refinement of the $2\theta$ values using the U−Fit program[20] yielded the values of the two a priori incommensurate parameters $\alpha = 0.33338(16)$ and $\beta = 0.27284(6)$. Subsequently three sets of data were collected: first for the main reflections, then the first-order satellite reflections, and finally second-order satellite reflections even though the latter had not been observed on the Buerger films. Table 1 lists the conditions of the data collection. The data were corrected for the scale variation, Lorentz-polarization effects, and absorption with the aid of several programs of the X-tal refinement package.[21] The averaging of symmetry related reflections was done according to the point symmetry of the different possible space groups. The internal agreement factors for the averaging of the reflections ($I \geq 2.5\sigma(I)$) were always between the values of 0.017 and 0.030. Some statistics regarding the different reflection classes are compiled in Table 2. The nonlinear least-squares refinements were performed using the JANA program[22] in the full-matrix mode, with unit weights for all reflections. The scattering factors for neutral atoms and the anomalous dispersion correction were taken from International Tables for X-ray Crystallography.

**Table 2. Reflection Statistics for Data Averaging in Super Space Group $C^{Pmmn\boldsymbol{a}}_{c\bar{m}\bar{m}1}$**

| | $N_1$ | $(I)$ | $I/\sigma(I)$ | $R_{int}$ | $N_2$ |
|---|---|---|---|---|---|
| main | 1411 | 606 | 27.0 | 0.019 | 434 |
| 1st order | 1183 | 58 | 9.0 | 0.037 | 536 |
| 2nd order | 334 | 16 | 4.9 | 0.053 | 226 |
| all | 2928 | 317 | 7.3 | 0.024 | 1196 |

[a] $N_1$ and $N_2$ refer to reflections with $I \geq 2.5\sigma(i)$. $N_1$ is the number of data collected. The total numbers of data collected were 1799 (main), 2864 (1st order), 3125 (2nd order), and 7788 (all). $N_2$ is the number of independent reflections left after averaging. Averaging in other superspace groups (i.e., without using an inversion center), affected $R_{int}$ only slightly, but the number of independent data increases drastically.

(11) Janssen, T.; Janner, A. *Adv. Phys.* **198**7, *36*, 519.
(12) Janssen, T.; Janner, A; Looyenga-Vos, A.; de Wolff, P. M. In *International Tables for Crystallography*; Kluwer Academic Publishers: Dordrecht, 1992; Vol. C, p 797.
(13) van Smaalen, S. *Cryst. Rev.* **1995**, *4*, 79.
(14) Pettifor, D. G.; Podloucky, R. *Phys. Rev. Lett.* **1984**, *53*, 1080.
(15) Burdett, J. K.; Lee, S. *J. Am. Chem. Soc.* **1985**, *107*, 3063.
(16) Lee, S.; Foran, B. *J. Am. Chem. Soc.* **1994**, *116*, 154.
(17) Hoistad, L. M.; Lee, S. *J. Am. Chem. Soc.* **1991**, *113*, 8216.
(18) Lee, S. *J. Am. Chem. Soc.* **1991**, *113*, 8216.
(19) Lee, S.; Rousseau, R.; Wells, C. *Phys. Rev. B* **1992**, *46*, 121.
(20) Evain, M. *U-FIT:* a cell parameter refinement program, Institut des Matériaux, Nantes, France, 1992.
(21) Hall, S. R.; Flack, H. D.; Stewart, J. M. *X-tal 3.2: Reference Manual*; Universities of Western Australia, Geneva, and Maryland, 1992.
(22) Petříček, V. *JANA93*: programs for modulated and composite crystals, Institute of Physics, Praha, Czech Republic, 1993.

## Symmetry and Refinement

**Average and Basic Structure.** The average structure has already been determined by Foran and Lee using main reflections only.[6] It is described in the tetragonal space group *P*4/*nmm* with three independent atoms, viz., Dy(1), Se(1), and Se(2) on the Wyckoff sites *2c* ($^1/_4$,$^1/_4$,0.73), *2c* ($^1/_4$,$^1/_4$,0.37), and *2a* ($^1/_4$,$^1/_4$,0), respectively. Dy(1) and Se(1) form a distorted NaCl-type framework between infinite two-dimensional square sheets formed by the Se(2) anions (Figure 1). The infinite Se(2) sheets are slightly depopulated. By using a sophisticated split model for Se(2) and anisotropic Debye−Waller parameters formally not allowed by the site symmetry, the authors obtained a final *R* factor of 0.020 (w*R* = 0.018). Although somewhat artificial, the model gives a clear indication of the displacive character of the modulation. The real modulation, however, can be determined only with the intensities of the satellite reflections. In addition, an eventual occupancy modulation in the Se(2) square sheets will only show up in the determination of the modulated structure.

Since the modulation wave vectors have orthorhombic symmetry, the basic structure is also necessarily orthorhombic, unlike the previously reported average structure. Note the difference between average and basic structure. The former is obtained by taking the average of all displacive and occupational deviations over one complete period of the modulation wave; experimentally it is determined by using only the main reflections in the refinement process. The basic structure, on the contrary, is obtained by setting all modulation amplitudes to zero. Thus, the modulated structure is equal to the sum of the basic structure plus the modulation.

The new measurements show that even the average structure is slightly orthorhombic, expressed in a small but significant length difference of the *a* and *b* axes, the angle $\gamma$ remaining 90° (Table 1). These observations, along with the modulation wave vector components ($\pm\alpha$,$\pm\beta$,$^1/_2$), lead to *Pmmn* or one of its subgroups as likely space group choices to describe the symmetry of both the average and basic structure. A refinement of the average structure parameters previously obtained by Foran and Lee in *Pmmn* yielded similar agreement factors (using the same $(\sin\theta/\lambda)_{max}$)[6] but did not give significant deviations that were indicative of a clear orthorhombic distortion. We therefore conclude that the average structure is tetragonal within a very good approximation. The refinement results with isotropic Debye−Waller parameters were used as a starting point for the determination of the modulated structure in order to avoid bias in the refinement of the displacive modulation amplitudes. The *R* factor of this model was 0.106 (w*R* = 0.114).

**Modulated Structure.** Not only the basic cell parameters but also the modulation parameters ($\pm\alpha$,$\pm\beta$, $^1/_2$) are slightly different from those previously reported. It should be noted that $\alpha$, within 1 standard deviation, is equal to the rational value $^1/_3$ and that $\beta$, within 2 standard deviations, is equal to $^3/_{11}$. Thus, the modulated structure could be described in a unit cell with a tripled *a*-axis, an 11-fold *b*-axis, and a doubled *c*-axis using standard crystallographic techniques. However, it is advantageous to use the superspace formalism for the refinement and analysis of such a large superstructure. The superspace formalism for modulated structures naturally divides the analysis into an average and a modulated part.[10,12] This division gives a smoother refinement process, often needing less independent parameters, and finally it also gives a direct link to the order parameters occurring in Landau theory.[23] In the present case the number of independent parameters can be reduced from 264 positional and 66 occupational parameters in a conventional supercell refinement to 33 positional and 5 occupational parameters (highest symmetry considered) using the superspace formalism.

Since there are two independent wave vectors $\mathbf{q}_1$ and $\mathbf{q}_2$, each spot of the diffraction pattern can be indexed with five integers ($h$,$k$,$l$,$m_1$,$m_2$). The symmetry of the structure is described with a (3+2)*D* superspace group. To analyze the systematic extinctions of the diffraction pattern, it is necessary to transform the basic unit cell in such a way that the symmetry-determined, rational components of the wavevector vanish. The required transformation is $\mathbf{a}' = \mathbf{a}$, $\mathbf{b}' = \mathbf{b}$, $\mathbf{c}' = 2\mathbf{c}$ which results in the new wavevector components ($\pm\alpha$,$\pm\beta$,0). The five reflection indexes transform accordingly to $H = h$, $K = k$, $L = 2l + m_1 + m_2$, $M_1 = m_1$, $M_2 = m_2$. The diffraction pattern now exhibits the general reflection condition $L + M_1 + M_2 = 2n$, corresponding to a centering translation vector of $(\mathbf{c} + \mathbf{a}_4 + \mathbf{a}_5)/2$, where $\mathbf{a}_4$ and $\mathbf{a}_5$ are the fourth and fifth unit vector respectively of the (3+2)*D* direct lattice. The reflection conditions corresponding to nonsymmorphic symmetry elements are $H + K = 2n$ and $H + K + M_1 + M_2 = 2n$ for ($HK0M_1M_2$) reflections. However, the latter condition, is already implied by the first and the centering condition. These conditions enable us to write the symbol of the (3+2)D superspace group as $C^{Pmmn}_{c\dot{m}\dot{m}1}$. Here the symbol *Pmmn* in the upper line represents the 3*D* space group of the (external) basic structure, and the symbol *cṁṁ1* in the bottom line the 2*D* space group that corresponds to the (internal) modulated part of the structure. The arrangement of the elements in the upper and lower lines is such that paired elements are on top of each other. The prefix *C* indicates the centering in internal space.

The matrix representation $\Gamma(R)$ of each (3+2)*D* symmetry operation *R* of the superspace group is determined by using $\Gamma_I(R)\sigma = \sigma\Gamma_E(R)$, where $\Gamma_E(R)$ is the (3 × 3) matrix representation corresponding to the rotational part of the (external) 3*D* symmetry operation of the basic structure, $\Gamma_I(R)$ is a (2 × 2) matrix acting on the fourth and fifth coordinate, and $\sigma$ is a (2 × 3) matrix whose rows are formed by the components of the two modulation wave vector. The (5 × 5) matrix $\Gamma(R)$ is then constructed from $\Gamma_E(R)$ and $\Gamma_I(R)$ by

$$\Gamma(R) = \begin{pmatrix} \Gamma_E(R) & 0 \\ 0 & \Gamma_I(R) \end{pmatrix} \qquad (1)$$

Table 3 lists all symmetry elements of $C^{Pmmn}_{c\dot{m}\dot{m}1}$, together with their associated external and internal translation vectors $\mathbf{v}_E$ and $\mathbf{v}_I$. It should be noted that because of the centering condition there are two symmetry elements of each kind in the unit cell that are

(23) Pérez-Mato, J. M.; Madaragia, G.; Tello, M. J. *Phys. Rev. B* **1983**, *30*, 1534.

**Table 3. Symmetry Elements of the Superspace Group $C_{c\dot{m}\dot{m}1}^{Pmmn}$ [a]**

| $(E_L,1\|n_1,n_2,n_3,n_4,n_5)$ | | $(E_C,1\|0,0,{}^1/_2,{}^1/_2,{}^1/_2)$ |
|---|---|---|
| | $(i,2\|0,0,0,0,0)$ | |
| $(2^x,\dot{m}\|{}^1/_2,0,0,0,0)$ | $(2^y,\dot{m}\|0,{}^1/_2,0,0,0)$ | $(2^z,2\|{}^1/_2,{}^1/_2,0,0,0)$ |
| $(m_x,\dot{m}\|{}^1/_2,0,0,0,0)$ | $(m_y,\dot{m}\|0,{}^1/_2,0,0,0)$ | $(m_z,1\|{}^1/_2,{}^1/_2,0,0,0)$ |

$$E_L=\begin{pmatrix}1&0&0\\0&1&0\\0&0&1\end{pmatrix}\quad E_C=\begin{pmatrix}1&0&0\\0&1&0\\0&0&1\end{pmatrix}\quad i=\begin{pmatrix}\bar1&0&0\\0&\bar1&0\\0&0&\bar1\end{pmatrix}$$

$$2^x=\begin{pmatrix}1&0&0\\0&\bar1&0\\0&0&\bar1\end{pmatrix}\quad 2^y=\begin{pmatrix}\bar1&0&0\\0&1&0\\0&0&\bar1\end{pmatrix}\quad 2^z=\begin{pmatrix}\bar1&0&0\\0&\bar1&0\\0&0&1\end{pmatrix}$$

$$m_x=\begin{pmatrix}\bar1&0&0\\0&1&0\\0&0&1\end{pmatrix}\quad m_y=\begin{pmatrix}1&0&0\\0&\bar1&0\\0&0&1\end{pmatrix}\quad m_z=\begin{pmatrix}1&0&0\\0&1&0\\0&0&\bar1\end{pmatrix}$$

$$1=\begin{pmatrix}1&0\\0&1\end{pmatrix}\quad 2=\begin{pmatrix}\bar1&0\\0&\bar1\end{pmatrix}\quad \dot{m}=\begin{pmatrix}0&1\\1&0\end{pmatrix}\quad \ddot{m}=\begin{pmatrix}0&\bar1\\\bar1&0\end{pmatrix}$$

[a] The (3+2)*D* symmetry element is designated $(R_E,R_I|\nu_1,\nu_2\nu_3,\nu_4,\nu_5)$, where $R_E$ and $R_I$ are represented by their respective symmetry symbols, $(\nu_1,\nu_2,\nu_3)$ is the external translation vector $\mathbf{v}_E$, and $(\nu_4,\nu_5)$ is the internal translation vector $\mathbf{v}_I$. All symmetry elements can be combined with the lattice translations $E_L$ or the centering translation $E_C$. The element $n_i$, $i = 1-5$, assumes all integer values.

similar in the average structure but different in the modulated structure. Therefore care must be taken in placing the unit cell contents with respect to these two symmetry elements.

Displacive modulation functions for all atoms and an occupational one for Se(2) were considered. The modulation functions are expanded in a Fourier series:

$$\mathbf{r}^\nu(\bar x_4,\bar x_5)=\mathbf{r}_0^\nu+\sum_{\substack{n_1,n_2=0\\n_1=n_2\neq0}}^{\infty,\infty}\{\mathbf{u}^\nu_{s,n1,n2}\sin[2\pi(n_1\bar x_4+n_2\bar x_5)]+\mathbf{u}^\nu_{c,n1,n2}\cos[2\pi(n_1\bar x_4+n_2\bar x_5)]\}\quad(2)$$

$$P^\nu(\bar x_4,\bar x_5)=P_0^\nu+\sum_{\substack{n_1,n_2=0\\n_1=n_2\neq0}}^{\infty,\infty}\{P^\nu_{s,n1,n2}\sin[2\pi(n_1\bar x_4+n_2\bar x_5)]+P^\nu_{c,n1,n2}\cos[2\pi(n_1\bar x_4+n_2\bar x_5)]\}\quad(3)$$

where $\nu$ counts the independent atoms in the basic unit cell. The arguments of the modulation functions are defined as follows:

$$\bar x_4=t_1+\mathbf{q}_1\cdot\mathbf{r}^\nu_{0,\mathrm{L}}=t_1+\mathbf{q}_1\cdot(\mathbf{r}_0^\nu+\mathbf{L})\quad(4)$$

$$\bar x_5=t_2+\mathbf{q}_2\cdot\mathbf{r}^\nu_{0,\mathrm{L}}=t_2+\mathbf{q}_2\cdot(\mathbf{r}_0^\nu+\mathbf{L})\quad(5)$$

where $t_1$ and $t_2$ are the global phases of the modulation waves ($t_1 = t_2 = 0$ is used in the present work), **L** is the basic structure lattice translations; $\mathbf{u}^\nu{}_{s,n1,n2} = (A^\nu{}_{x,s,n1,n2}, A^\nu{}_{y,s,n1,n2}, A^\nu{}_{z,s,n1,n2})$ and $\mathbf{u}^\nu{}_{c,n1,n2} = (A^\nu{}_{x,c,n1,n2}, A^\nu{}_{y,c,n1,n2}, A^\nu{}_{z,c,n1,n2})$. Only the waves $(n_1,n_2) = (1,0)$, $(0,1)$, $(2,0)$, $(0,2)$, $(1,1)$, and $(1,-1)$ were taken into account, since only satellite reflections up to the second order have been observed.

All three independent atoms have the same site symmetry. The modulation functions have to be invariant under the generating symmetry elements, $m_x$ and $m_y$. Table 4 lists the restrictions on the Fourier amplitudes that follow from this invariance condition. The subgroups of $C_{c\dot{m}\dot{m}1}^{Pmmn}$ that were also considered in the refinements are $C_{c\dot{m}\dot{m}1}^{Pm2_1n}$, $C_{c\dot{m}\dot{m}1}^{P2_1mn}$, $C_{c\dot{m}\dot{m}2}^{Pmm2}$, and $C_{c\dot{m}\dot{m}1}^{P2_12_12}$. These subgroups have different symmetry restrictions since the atoms, in general, are on sites with lower symmetry.

The refinements proceeded as follows. The first-order Fourier amplitude of the occupancy wave of Se(2), $P^{\mathrm{Se}(2)}_{\mathrm{c},1,0}$, was given a small but significant value, e.g., 0.10. All first-order Fourier amplitudes were then refined in 5−10 iteration cycles using only the intensities of first-order satellites. Other parameters were kept fixed. Next the obtained refinement minimum was tested against a reversal of the signs of arbitrarily chosen displacive Fourier amplitudes. The possibility of a lower *R* factor by using −0.10 as a starting value for $P^{\mathrm{Se}(2)}_{\mathrm{c},1,0}$ was also verified. The most satisfactory solution was then used for further refinements. The basic structure parameters were refined using only the main reflections. This was followed by a combined refinement of all basic parameters and first-order Fourier amplitudes using main plus first-order satellite reflections. At the end of this stage the *R* factors were generally about 0.06 for the main reflections and 0.13 for the first-order satellites. Finally the second-order satellite reflections were added to the refinement process for the determination of all parameters, including the second-order Fourier amplitudes.

In the five tested models anisotropic Debye−Waller parameters for all atoms and an extinction parameter were refined. All the models gave comparable *R* factors, except the model in $C_{c\dot{m}\dot{m}1}^{P2_1mn}$, where large correlations hampered a smooth convergence. To decide which models were preferable, interatomic distances in the 3**a** × 11**b** × 2**c** supercell were calculated. The $C_{c\dot{m}\dot{m}1}^{P2_1mn}$ model was then rejected because of unrealistically short Se(2)−Se(2) distances (<2.0 Å). Table 5 compiles the agreement factors of the remaining four models I−IV. Table 6 gives the refinement results of the best model, $C_{c\dot{m}\dot{m}1}^{P2_1mn}$ (vide infra). Structure factor tables and refinement information of the other models may be obtained upon request from the authors.

**Interpretation of the Occupancy Wave of Se(2).** Figure 2 shows the occupancy modulation function of Se(2), found for space group $C_{c\dot{m}\dot{m}1}^{P2_1mn}$, model II, plotted against the two phase parameters $t_1$ and $t_2$. A steep minimum at $\sim(t_1,t_2) = (0.8,0.1)$ is observed, whereas a similar steep maximum is absent. Minimal and maximal function values are slightly below 0.0 and above 1.0, respectively. These nonphysical occupancy values are obtained because the modulation functions were expanded only up to the second order. Other examples have shown that functions describing large occupational modulations are of the block wave type with amplitude 1.[24,25] In other words, sites are empty or occupied. Limiting the Fourier expansion to a few harmonics

(24) van der Lee, A.; van Smaalen, S.; Wiegers, G. A.; de Boer, J. L. *Phys. Rev. B* **1991**, *43*, 9420.
(25) van der Lee, A.; Monconduit, L.; Brec, R.; Rouxel, J.; Petříček, V. *Acta Crystallogr. B* **1994**, *50*, 119.

**Table 4. Symmetry Restrictions for Superspace Group**

| $m_x$ | $m_y$ | $2^z$ | $mm2$ |
|---|---|---|---|
| $P^{\nu}_{s,n1,0} = -P^{\nu}_{s,0,n1}$ | $P^{\nu}_{s,n1,0} = P^{\nu}_{s,0,n1}$ | $P^{\nu}_{s,n1,0} = -P^{\nu}_{s,0,n1}$ | $P^{\nu}_{s,n1,0} = P^{\nu}_{s,0,n1} = 0$ |
| $P^{\nu}_{c,n1,0} = P^{\nu}_{c,0,n1}$ | $P^{\nu}_{c,n1,0} = P^{\nu}_{c,0,n1}$ | $P^{\nu}_{c,n1,0} = P^{\nu}_{c,0,n1}$ | $P^{\nu}_{c,n1,0} = P^{\nu}_{c,0,n1}$ |
| $P^{\nu}_{s,n1,n1} = 0$ | $P^{\nu}_{s,n1,n1}$ | $P^{\nu}_{s,n1,n1} = 0$ | $P^{\nu}_{s,n1,n1} = 0$ |
| $P^{\nu}_{c,n1,n1}$ | $P^{\nu}_{c,n1,n1}$ | $P^{\nu}_{c,n1,n1}$ | $P^{\nu}_{c,n1,n1}$ |
| $P^{\nu}_{s,n1,-n1}$ | $P^{\nu}_{s,n1,-n1} = 0$ | $P^{\nu}_{s,n1,-n1} = 0$ | $P^{\nu}_{s,n1,-n1} = 0$ |
| $P^{\nu}_{c,n1,-n1}$ | $P^{\nu}_{c,n1,-n1}$ | $P^{\nu}_{c,n1,-n1}$ | $P^{\nu}_{c,n1,-n1}$ |
| $A^{\nu}_{x,s,n1,0} = A^{\nu}_{x,s,0,n1}$ | $A^{\nu}_{x,s,n1,0} = A^{\nu}_{x,s,0,n1}$ | $A^{\nu}_{x,s,n1,0}$, $A^{\nu}_{x,s,0,n1}$ | $A^{\nu}_{x,s,n1,0} = A^{\nu}_{x,s,0,n1}$ |
| $A^{\nu}_{x,c,n1,0} = -A^{\nu}_{x,c,0,n1}$ | $A^{\nu}_{x,c,n1,0} = A^{\nu}_{x,c,0,n1}$ | $A^{\nu}_{x,c,n1,0} = A^{\nu}_{x,c,0,n1} = 0$ | $A^{\nu}_{x,c,n1,0} = A^{\nu}_{x,c,0,n1} = 0$ |
| $A^{\nu}_{y,s,n1,0} = -A^{\nu}_{y,s,0,n1}$ | $A^{\nu}_{y,s,n1,0} = -A^{\nu}_{y,s,0,n1}$ | $A^{\nu}_{y,s,n1,0}$, $A^{\nu}_{y,s,0,n1}$ | $A^{\nu}_{y,s,n1,0} = -A^{\nu}_{y,s,0,n1}$ |
| $A^{\nu}_{y,c,n1,0} = A^{\nu}_{y,c,0,n1}$ | $A^{\nu}_{y,c,n1,0} = -A^{\nu}_{y,c,0,n1}$ | $A^{\nu}_{y,c,n1,0} = A^{\nu}_{y,c,0,n1} = 0$ | $A^{\nu}_{y,c,n1,0} = A^{\nu}_{y,c,0,n1} = 0$ |
| $A^{\nu}_{z,s,n1,0} = A^{\nu}_{z,s,0,n1}$ | $A^{\nu}_{z,s,n1,0} = A^{\nu}_{z,s,0,n1}$ | $A^{\nu}_{z,s,n1,0} = A^{\nu}_{z,s,0,n1} = 0$ | $A^{\nu}_{z,s,n1,0} = A^{\nu}_{z,s,0,n1} = 0$ |
| $A^{\nu}_{z,c,n1,0} = A^{\nu}_{z,c,0,n1}$ | $A^{\nu}_{z,c,n1,0} = A^{\nu}_{z,c,0,n1}$ | $A^{\nu}_{z,c,n1,0}$, $A^{\nu}_{z,c,0,n1}$ | $A^{\nu}_{z,c,n1,0} = A^{\nu}_{z,c,0,n1}$ |
| $A^{\nu}_{x,s,n1,n1}$ | $A^{\nu}_{x,s,n1,n1}$ | $A^{\nu}_{x,s,n1,n1}$ | $A^{\nu}_{x,s,n1,n1}$ |
| $A^{\nu}_{x,c,n1,n1} = 0$ | $A^{\nu}_{x,c,n1,n1}$ | $A^{\nu}_{x,c,n1,n1} = 0$ | $A^{\nu}_{x,c,n1,n1} = 0$ |
| $A^{\nu}_{y,s,n1,n1} = 0$ | $A^{\nu}_{y,s,n1,n1} = 0$ | $A^{\nu}_{y,s,n1,n1}$ | $A^{\nu}_{y,s,n1,n1} = 0$ |
| $A^{\nu}_{y,c,n1,n1}$ | $A^{\nu}_{y,c,n1,n1} = 0$ | $A^{\nu}_{y,c,n1,n1} = 0$ | $A^{\nu}_{y,c,n1,n1} = 0$ |
| $A^{\nu}_{z,s,n1,n1} = 0$ | $A^{\nu}_{z,s,n1,n1}$ | $A^{\nu}_{z,s,n1,n1} = 0$ | $A^{\nu}_{z,s,n1,n1} = 0$ |
| $A^{\nu}_{z,c,n1,n1}$ | $A^{\nu}_{z,c,n1,n1}$ | $A^{\nu}_{z,c,n1,n1}$ | $A^{\nu}_{z,c,n1,n1}$ |
| $A^{\nu}_{x,s,n1,-n1} = 0$ | $A^{\nu}_{x,s,n1,-n1} = 0$ | $A^{\nu}_{x,s,n1,-n1}$ | $A^{\nu}_{x,s,n1,-n1} = 0$ |
| $A^{\nu}_{x,c,n1,-n1} = 0$ | $A^{\nu}_{x,s,n1,-n1}$ | $A^{\nu}_{x,s,n1,-n1} = 0$ | $A^{\nu}_{x,s,n1,-n1} = 0$ |
| $A^{\nu}_{y,s,n1,-n1}$ | $A^{\nu}_{y,s,n1,-n1}$ | $A^{\nu}_{y,s,n1,-n1}$ | $A^{\nu}_{y,s,n1,-n1}$ |
| $A^{\nu}_{y,c,n1,-n1}$ | $A^{\nu}_{y,s,n1,-n1} = 0$ | $A^{\nu}_{y,s,n1,-n1} = 0$ | $A^{\nu}_{y,s,n1,-n1} = 0$ |
| $A^{\nu}_{z,s,n1,-n1}$ | $A^{\nu}_{y,c,n1,-n1}$ | $A^{\nu}_{y,c,n1,-n1} = 0$ | $A^{\nu}_{y,c,n1,-n1} = 0$ |
| $A^{\nu}_{z,c,n1,-n1}$ | $A^{\nu}_{z,c,n1,-n1}$ | $A^{\nu}_{z,c,n1,-n1}$ | $A^{\nu}_{z,c,n1,-n1}$ |

**Table 5. Final Agreement Factors for the Refinements of Models I–IV**

| | overall | | | main | | | first-order | | | second-order | | | | |
|---|---|---|---|---|---|---|---|---|---|---|---|---|---|---|
| | $R$ | $R_w$ | $N_{ref}$ | $R$ | $R_w$ | $N_{ref}$ | $R$ | $R_w$ | $N_{ref}$ | $R$ | $R_w$ | $N_{ref}$ | $n_p$ | $n_o$ |
| I | 0.068 | 0.063 | 1196 | 0.037 | 0.041 | 434 | 0.102 | 0.127 | 536 | 0.230 | 0.289 | 226 | 33 | 5 |
| II | 0.054 | 0.051 | 1606 | 0.037 | 0.039 | 758 | 0.088 | 0.109 | 601 | 0.190 | 0.245 | 247 | 60 | 8 |
| III | 0.059 | 0.055 | 2045 | 0.034 | 0.036 | 811 | 0.089 | 0.110 | 944 | 0.243 | 0.300 | 290 | 66 | 10 |
| IV | 0.059 | 0.057 | 1913 | 0.037 | 0.040 | 685 | 0.081 | 0.106 | 944 | 0.193 | 0.244 | 284 | 58 | 7 |

[a] The definitions of the $R$ factors are $R = \sum||F_{obs}| - |F_{cal}||/\sum|F_{obs}|$ and $wR = [\sum w(|F_{obs}| - |F_{cal}|)^2/\sum w|F_{obs}|^2]^{1/2}$, with unit weights $w = 1$. $N_{ref}$ is the number of reflections with $I \geq 2.5\sigma(I)$ for each reflection class that is used in the refinements. $n_p$ is the number of positional parameters, and $n_o$ is the number of occupational parameters. The models I–IV correspond to the superspace groups $C^{Pmmn}_{c\dot{m}\dot{m}1}$, $C^{Pm2_1n}_{c\dot{m}\dot{m}1}$, $C^{Pmm2}_{c\dot{m}\dot{m}2}$, and $C^{P2_12_12}_{c\dot{m}\dot{m}2}$, respectively.

necessarily leads to the mathematical phenomena of "under-" and "overshoot". We took $P(Se(2)) = {}^1/_2$ as a cutoff criterion to decide whether a site is occupied or not; above this cutoff the site is regarded as occupied, below ${}^1/_2$ it is empty. In this way, mean occupancies close to the refined values were obtained.

**In-Plane Se Distributions.** Figure 3 illustrates the distorted square-nets of the four best solutions from the structure refinements in a 3**a** × 11**b** planar cell. Shown are the Se(2) distributions projected onto the $z = 0$ plane (there are only slight displacements out of this plane). The solid lines represent Se(2)–Se(2) distances between 2.1 and 2.5 Å and the dashed lines represent distances between 2.5 and 2.8 Å. The remainder of the structure, i.e., the distorted NaCl arrangement of Dy and Se(1) between the successive Se(2) sheets is discarded for the moment, since its modulation is much weaker than that of the Se(2) sheet.

The $C^{Pmmn}_{c\dot{m}\dot{m}1}$ (Figure 3a, hereafter model I) and the $C^{Pm2_1n}_{c\dot{m}\dot{m}1}$ (Figure 3b, hereafter model II)) solutions are quite similar: in both cases vacant Se(2) sites are grouped together in pairs. Vacancy pairs are not found in the other known rare-earth selenides. The essential difference between the two models are two 90° rotated Se–Se pairs. Model III, superspace group $C^{P2_1mn}_{c\dot{m}\dot{m}1}$ (Figure 3c), is less attractive than the first two models, since it contains much shorter Se–Se distances of about 2.18 Å, to be compared with the 2.38 Å distances in models I and II. The latter correspond with $(Se–Se)^{2-}$ pairs found in many other selenides. Another distinguishing feature is that the vacancy pairs of model I and II are absent. However, the single-vacancy sites of model III are similar to other patterns of rare-earth selenides. Model IV, superspace group $C^{P2_12_12^2}_{c\dot{m}\dot{m}1}$ (Figure 3d), is comparable with the models I and II regarding the shortest Se–Se distances and the occurrence of vacancy pairs. Using the criterium of the shortest Se–Se bond distances, model III is clearly an inferior model with bond distances less than 2.3 Å. Therefore, we have focused our following theoretical study on the three remaining models, I, II and IV.

## Discussion Based on Crystallographic Data

The very strongly displacive modulation wave of the Se(2) atoms may be attributed to the contributions from these atoms to electronic states near the Fermi level which are most affected by the CDW. The in-plane ($a$–$b$) modulation is much stronger than the modulation

**Table 6. Final Refinement Results for Model II (Superspace Group $C_{cm\bar{m}1}^{Pm2_1n}$)[a]**

| atom $\nu$ | Dy | Se(1) | Se(2) |
|---|---|---|---|
| $x$ | 0.25(*) | 0.25(*) | 0.25(*) |
| $y$ | 0.25(*) | 0.258(1) | 0.760(3) |
| $z$ | 0.36355(4) | 0.18402(7) | 0.0007(6) |
| $A^{\nu}_{x,s,1,0}$ | 0.0028(6) | −0.0032(6) | −0.055(2) |
| $A^{\nu}_{y,s,1,0}$ | 0.0058(4) | −0.0044(9) | −0.043(2) |
| $A^{\nu}_{z,s,1,0}$ | −0.0015(7) | −0.0002(5) | 0.0015(5) |
| $A^{\nu}_{x,c,1,0}$ | 0.0057(7) | 0.003(1) | 0.013(6) |
| $A^{\nu}_{y,c,1,0}$ | 0.0003(10) | 0.007(2) | 0.002(6) |
| $A^{\nu}_{z,c,1,0}$ | 0.0065(2) | 0.0039(1) | 0.0022(6) |
| $A^{\nu}_{x,s,2,0}$ | −0.0012(7) | −0.002(3) | −0.0004(30) |
| $A^{\nu}_{y,s,2,0}$ | 0.002(1) | 0.008(2) | −0.010(3) |
| $A^{\nu}_{z,s,2,0}$ | −0.0007(3) | 0.0021(5) | 0.0003(7) |
| $A^{\nu}_{x,c,2,0}$ | 0.0008(8) | 0.012(2) | 0.013(3) |
| $A^{\nu}_{y,c,2,0}$ | 0.004(1) | −0.0006(30) | −0.013(3) |
| $A^{\nu}_{z,c,2,0}$ | 0.0008(2) | 0.0010(5) | 0.0022(4) |
| $A^{\nu}_{y,s,1,1}$ | 0.0044(9) | −0.001(2) | −0.024(4) |
| $A^{\nu}_{z,s,1,1}$ | −0.0004(5) | 0.0008(6) | −0.0025(7) |
| $A^{\nu}_{y,c,1,1}$ | 0.003(2) | −0.002(3) | 0.017(6) |
| $A^{\nu}_{z,c,1,1}$ | −0.0022(2) | −0.0002(3) | 0.0007(6) |
| $A^{\nu}_{x,s,1,-1}$ | 0.0035(7) | −0.001(1) | −0.022(2) |
| $A^{\nu}_{y,c,1,-1}$ | −0.002(2) | −0.003(3) | 0.013(4) |
| $A^{\nu}_{z,c,1,-1}$ | −0.0018(2) | −0.0001(3) | 0.0024(5) |
| $P^{\nu}_{0}$ | 1.0000 | 1.00000 | 0.794(8) |
| $P^{\nu}_{s,1,0}$ | 0.0000 | 0.0000 | −0.06(3) |
| $P^{\nu}_{c,1,0}$ | 0.0000 | 0.0000 | −0.23(1) |
| $P^{\nu}_{s,2,0}$ | 0.0000 | 0.0000 | −0.01(2) |
| $P^{\nu}_{c,2,0}$ | 0.0000 | 0.0000 | −0.03(2) |
| $P^{\nu}_{s,1,1}$ | 0.0000 | 0.0000 | −0.10(5) |
| $P^{\nu}_{c,1,1}$ | 0.0000 | 0.0000 | −0.15(3) |
| $P^{\nu}_{c,1,-1}$ | 0.0000 | 0.0000 | −0.10(2) |

[a] Standard deviation are within parentheses. The *y*-coordinate of Dy was kept fixed to define the origin along the *b*-axis.

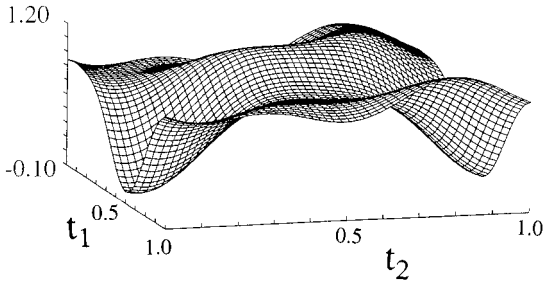


**Figure 2.** Occupational modulation wave of Se(2) for model II, superspace group $C_{cm\bar{m}1}^{Pm2_1n}$ as a function of the two phase parameters $t_1$ and $t_2$.

perpendicular to the $a-b$ plane. Although the average Se(2)−Se(2) distance is 2.833 Å, the real modulated structure shows Se(2)−Se(2) distances ranging from 2.37 to about 3.45 Å. The shortest distances, 2.375 and 2.382 Å, compare well with those found, e.g., in elemental Se (2.37 Å)[26] and $A_2Se_3$ ($A$ = K, Rb, Cs; 2.36−2.38 Å).[27] Shortest distances in other rare-earth selenides are somewhat longer: 2.48 Å in $La_{10}Se_{19}$[5] and 2.45 Å in $LaSe_2$.[28] Figure 4 shows a histogram of Se(2)−Se(2) distances in the square sheet. Distances primarily cluster around 2.40 and 2.95 Å, although intermediate and longer distances are also present. The short distances represent $Se_2^{2-}$, whereas the longer distances are assigned to higher polyselenide ions $Se_n^{m-}$. We thus observe the effect of the CDW modulation as the formation of selenium−selenium bonds.

The in-plane modulation of Dy and Se(1) is in general a factor 5−10 times smaller than that of Se(2). The modulation in the *c* direction is greater for Dy than for both Se atoms, viz. about 0.053 Å. These displacements are nicely correlated to the Se(2)−Se(2) pair formation in the infinite square sheets. The Dy atoms projected onto the Se(2) sheets are approximately squarely coordinated by the Se(2) atoms, more precisely by the Se(2) sites whether occupied or not. If the projected Dy atom is close to a Se(2)−Se(2) pair, it tends to shift away from the infinite square sheet, thus toward the distorted NaCl layer. On the contrary, if the Se(2) atoms making up the square around Dy are not paired, the Dy atoms moves toward the Se(2) sheet, away from the NaCl layer. This type of correlation is reminiscent of that found in another two-dimensional occupationally modulated structure, $Ag_{0.6}NbS_2$,[24] in which S atoms (of $NbSe_2$ layers) move toward empty Ag sites in adjacent layers forming slightly puckered 2D honeycomb shaped lattices of Ag. The Se(1) displacive modulation is not directly linked to the occupational distribution of Se(2) since it is farther away from the infinite sheets.

The block wave character of the occupational modulation gives rise to either occupied or empty sites. The final model has 2 vacant sites out of every 11 sites in the square sheets, to be compared with, for instance, one vacancy out of every 10 sites in the case of $Ce_{10}Se_{19}$ and $Pr_{10}Se_{19}$.[5] The observed Se deficiency may be the very reason for the orthorhombic symmetry of the modulated structure, since there is no tetragonal supercell compatible with a $Dy_{11}Se_{20}$ stoichiometry.

Much of the three model structures can be understood through the VSEPR (valence shell electron pair repulsion) rules.[29] In the VSEPR system of electron counting one may assign fixed numbers of valence electrons to particular coordination geometries. An isolated Se atom is assumed to have eight valence electrons. A selenium atom coordinated to only one other Se is assigned seven valence electrons, while a two-coordinate selenium atom has eight valence electrons if the coordination is linear and six valence electrons if bent. Thus an $Se_2$ dimer has two one-coordinate Se atoms and hence a total of 14 valence electrons. If we recall that a neutral Se atom has six valence electrons, we may denote such a $Se_2$ dimer as $[Se_2]^{2-}$ ($14 - 2 \times 6 = 2$).

We apply these VSEPR electron counting rules to the structure of $Dy_{11}Se_{20}$ in the following manner. First, let us assume that all Se−Se distances shown in Figure 3 correspond to Se−Se bonds; these correspond to all those made shorter by the charge density wave modulation. The defective square lattice is thus fragmented into molecular anionic selenium clusters. Following the VSEPR method of electron counting, to each of these clusters, we may assign a fixed number of electrons. In the case of model I for example the overall square lattice

(26) Donohue, J. *The Structure of the Elements*; Wiley: New York, 1974; p 317.
(27) Böttcher, P. *Z. Anorg. Allg. Chem.* **1977**, *432*, 167. Böttcher, P. *Ibid.* **1980**, *461*, 13.
(28) Bénazeth, S.; Carré, D.; Laruelle, P. *Acta Crystallogr. B* **1982**, *38*, 33.
(29) Cotton, F. A.; Wilkson, G. *Advanced Inorganic Chemistry*, 4th ed.; Wiley-Interscience: New York, 1980; p 196.

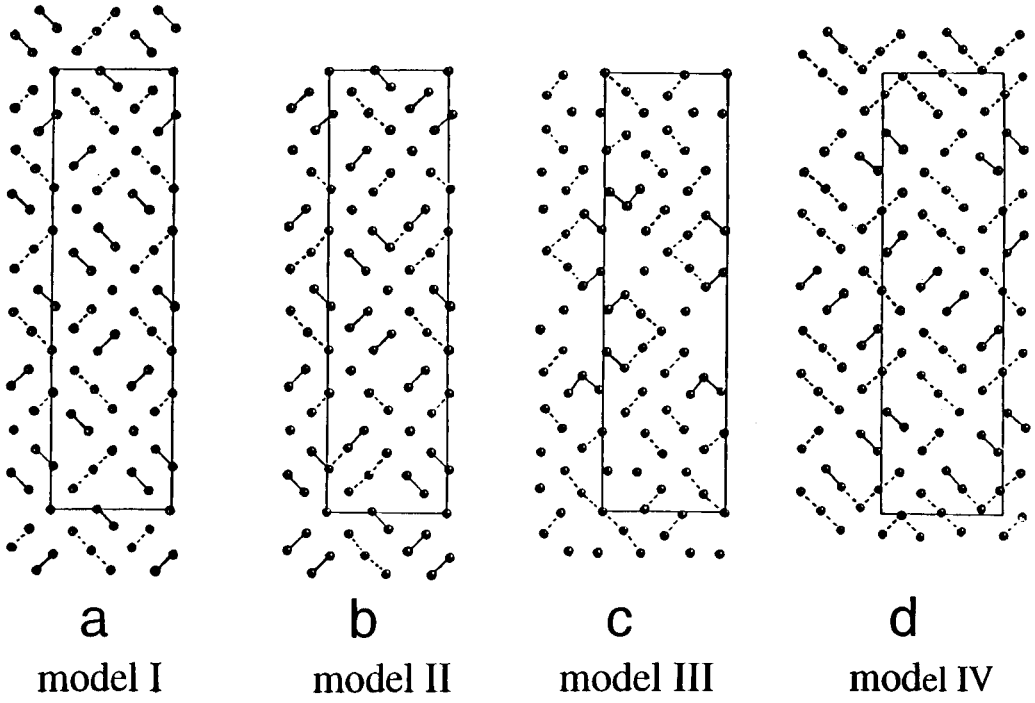


**Figure 3.** In-plane Se(2) distribution for the models of (a) $C_{c\bar{m}\bar{m}1}^{Pm2_1n}$, model I, (b) $C_{c\bar{m}\bar{m}1}^{Pm2_1n}$, model II, (c) $C_{c\bar{m}\bar{m}1}^{Pm2_1n}$, model III, and (d) $C_{c\bar{m}\bar{m}1}^{Pm2_1n}$, model IV. Solid lines represent Se(2)−Se(2) distances between 2.1 and 2.5 Å, dashed lines represent distances between 2.5 and 2.8 Å.

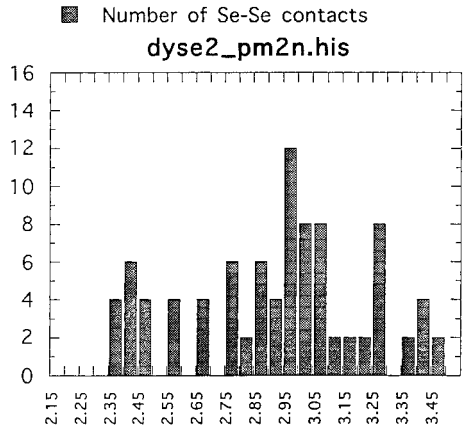


**Figure 4.** Number of Se(2)−Se(2) contacts in the $z = 0$ plane as a function of contact distance.

contains per unit cell 4 isolated $Se^{2-}$ atoms, 16 $Se_2^{2-}$ dimers, and 6 linear $Se_3^{4-}$ trimers. Considering the full contents of the unit cell [for which the formula unit is $Dy_{132}Se_{240}$] the total charge of the Se atoms is −392.[30] If each Dy atom assumes the oxidation state of +3, then we find a total positive charge of +396, which is within 1% of the calculated charge for the Se atoms given above.

This result is particularly important for the following reason. In the three models with chemically reasonable bond distances (models I, II, and IV) it turns out that in every case such electron counting results in an overall charge of −392. This is true irrespective of whether we assume the minimum distance for a Se−Se bond is 2.8 Å or whether the minimum distance is 2.7 Å. We therefore conclude that this agreement between the selenium lattice and the dysprosium oxidation state is not fortuitous. Indeed it should be noted that one possibility for the slight mismatch between the selenium and dysprosium charge is a slight nonstoichiometry in either selenium or dysprosium. Such a nonstoichiometry would be of a value too small to detect with X-ray crystallography. It would correspond to an approximate 1% change in Dy or Se composition. To emphasize this possibility we note that stoichiometries such as $Dy_{65.33}Se_{120}$ are plausible and provide perfect charge neutrality.

## Calculational Method

For the energy we use the second moment scaled Hückel method where

$$E_{TOT} = \int_{E_F}^{-\infty} E\rho(E)\,dE + \gamma \int_{\infty}^{-\infty} E^2\rho(E)\,dE$$

In this formula $E_F$ is the Fermi level, $\rho(E)$ is the tight-binding density of states, and $\gamma$ is a constant determinable from experimental equilibrium size. This is a minimal basis set calculation using Slater type orbitals with a single-$\zeta$ expansion, and the unweighted Wolfsberg−Helmholz approximation[32] for off-diagonal matrix elements, i.e., $H_{ij} = KS_{ij}(H_{ii} + H_{ij})$. The parameters used to describe the energy and the shape of the basis orbitals for selenium are those optimized to account for the contracted s orbitals, as discussed in refs 16 and 31. Dysprosium atoms are assumed to donate three valence electrons to the selenium. The $\mu_2$-Hückel method has been previously applied to account for electron counting rules such as Wade's rules for electron-

(30) In arriving at this electron count, we have included the 132 Se atoms which do not form part of the defective square lattice shown in Figure 5. However, for these latter Se atoms, as they lie at a distance of 3.54 Å away from all other Se atoms, it is clear that by VSEPR that they should be considered $Se^{2-}$ monomeric atoms.

(31) Hoffmann, R.; Shaik, S.; Scott, J. C.; Whangbo, M.-H.; Foshee, M. J. *J. Solid State Chem.* **1980**, *34*, 263.
(32) Wolfsberg, M.; Helmholz, L. *J. Chem. Phys.* **1957**, *20*, 83.

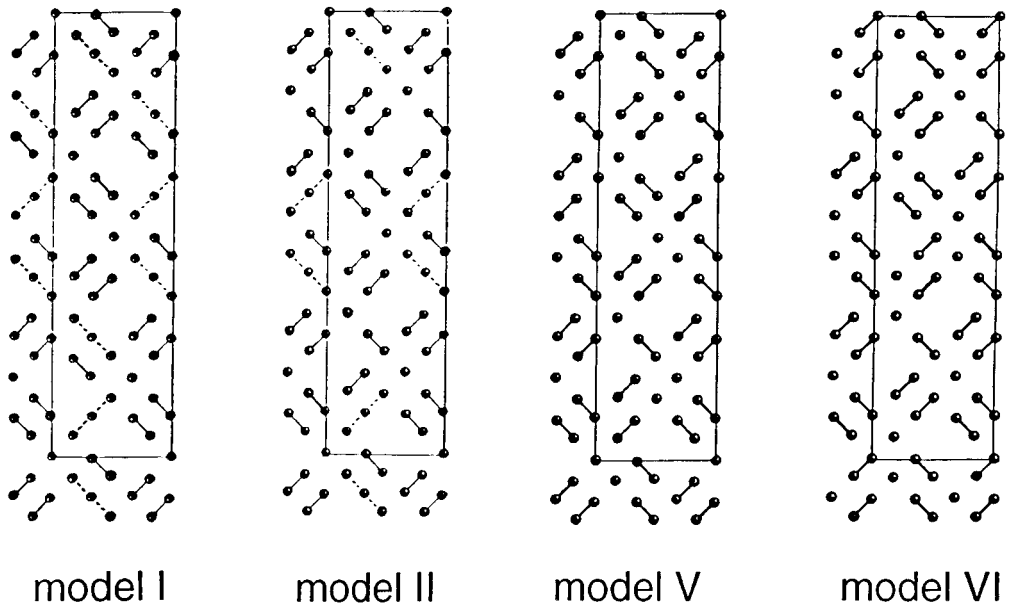


**Figure 5.** Idealized structures for calculation of second-moment scaled Hückel energies: (a) model I, (b) model II, (c) model V, and (d) model VI. Solid lines represent Se(2)−Se(2) distances between 2.1−2.5 Å, dashed lines represent distances between 2.5 and 2.8 Å.

deficient clusters, the Hume−Rothery rules for noble- and transition-metal alloys, and the octet rule of main-group compounds. We have further used this method to produce optimal energy structures for both solids and molecules that are in reasonable agreement with experiment. Systems studied include solids such as elemental boron, zinc, gallium, manganese, $LaSe_2$, $La_{10}Se_{19}$, and $RbDy_3Se_8$ and molecules such as boranes, carboranes, simple hydrocarbons, phosphorus−sulfur clusters, and transition-metal carbonyl clusters.[16−19]

**$\mu_2$-Hückel Results.** We used the $\mu_2$-Hückel method to directly compare the energies of the three proposed models. In doing so some care must be taken. The precise location of the atoms are not known; therefore, any direct energetic comparison may result only in assessing the accuracy of bond lengths in a given model rather than an evaluation of the correctness of the overall distortion patterns. We therefore carried out a calculation on an idealized structure which minimizes errors due to incorrect bond lengths. Starting from the ideal square lattice, we allowed atoms either to shift a distance of 0.37 Å along the Se−Se bond directions or to stay in their ideal position. We then chose the patterns that most closely resembled the true structures of models I, II, and IV. The idealized structures of models I and II are shown in Figure 5. It may be seen that they are in reasonable agreement with the models from the X-ray determination. We found that the energies of models I, II, and IV are respectively −17 890.1, −17 891.5, and −17 888.0 eV. These results suggest that model II is the lowest energy structure.

This energy difference is in accord with our earlier work on smaller supercells in related rare-earth selenides. In these earlier studies we found that the energetically preferred structure was always one in which HOMO−LUMO (highest occupied and lowest unoccupied molecular orbitals) interactions between neighboring selenide fragments was maximized. This principle of maximal frontier overlap is a well-known general rule whenever interactions are strong and


**Figure 6.** Principle unfilled molecular orbitals, $\sigma^*$, found for the ions $Se_3^{4-}$ and $Se_2^{2-}$.

covalent as is found in these systems.[33,34] In the case of the rare-earth selenides, there are relatively few unfilled fragment orbitals. The principle of maximum overlap therefore reduces to one of minimization of all unoccupied-to-unoccupied orbital interactions. In models I, II and IV the principal unfilled molecular orbitals are the $\sigma^*$ orbitals found in linear $Se_3^{4-}$ and $Se_2^{2-}$ clusters. These orbitals are illustrated in Figure 6. In model I for example it can be seen that there are pairs of linear $Se_3^{4-}$ trimers that lie in a coaxial arrangement to one another (see Figures 3 and 5). As the LUMO orbitals on $Se_3^{4-}$ are $\sigma^*$ orbitals pointed along the axis of the $Se_3^{4-}$ molecular axis, one finds that the coaxial $Se_3^{4-}$ arrangement found in models I and IV lead to a LUMO−LUMO interaction rather than a pure LUMO−HOMO interaction. Such interactions are unfavorable. By contrast, in model II, all LUMOs are in direct overlap with neighboring HOMO orbitals. This fact is a significant factor in the stability of model II.

While the results of our theoretical calculations rule out models I and IV, these do not prove that model II is the correct crystallographic structure. One possible change in model II is to break the linear $Se_3^{4-}$ trimers into a monomeric $Se^{2-}$ and an $Se_2^{2-}$ dimer. Similarly we can break the check-shaped $Se_4^{4-}$ tetramers shown in Figure 3b into two $Se_2^{2-}$ dimers. Such a change leaves all LUMOs pointed directly to HOMOs. Our calculations show that a model with such distortions allows a further stabilization of the energy of the system. Thus the lowest energy distortion patterns we

(33) Burdett, J. K. *Chemical Bonding in Solids*; Oxford Press: New York, 1955.
(34) Hoffmann, R. *Solids and Surfaces: A Chemist's View on Bonding in Extended Structures*; VCH Publishers, Inc.: New York, 1988.

have found are those of model V and VI shown in Figure 5. We find models V and VI have electronic energies respectively of −17 892.86 and −17 892.92 eV, 1.4 eV lower in $\mu_2$-Hückel energy than the model II structure. Model V is also a resultant structure if one replaces all the trimers of model I by monomer-plus-dimer combinations. Model V thus lies on a direct pathway between models I and II, while model VI involves a combination of elements from both models I and II. As models V and VI are rather close to the previous models, the crystallographic data are not by itself sufficient to resolve one way or another the validity of these models over the other models.

The principal difference between the lower energy theoretically generated models V and VI and the experimentally determined models I−IV are an absence of any linear $Se_3^{4-}$ fragments in the former systems. As to our knowledge, there are no known linear $Se_3^{4-}$ units in the selenide crystal chemistry literature, we believe that the energy difference may indeed be significant.

The present study has shown that a combination of advanced crystallographic analysis and second-moment scaled, tight-binding, band calculations is very useful in solving a complex modulated structure like $DySe_{1.84}$. The X-ray analysis resulted in three different models with chemically reasonable bond distances and comparable agreement factors. These three models were, somewhat idealized, used as a starting point for the band calculations. The calculations suggested that the real structure should be somewhere between two of the proposed X-ray models. The lowest energy structure could be understood using simple HOMO−LUMO interaction arguments: the higher the interactions between neighboring selenide fragments throughout the structure, the lower the energy.

**Acknowledgment.** The research of A.v.d.L. has been made possible by a grant from the CNRS (Sciences Chimiques) and that of L.M.H. by a grant from the Conseil Général des Pays de la Loire. The work of B.J.F. and S.L. was supported by funds from the U.S. Petroleum Research Fund and NSF (DMR-9319196). In addition S.L. would like to thank the A.P. Sloan Foundation, the J.D. and C.T. MacArthur Foundation, and the Alexander von Humboldt Foundation for fellowships. We would also like to thank Prof. Jean Rouxel for his thoughtful comments.

CM960302T